

Internal Conversion Rates from the Extended Thawed Gaussian Approximation: Theory and Validation

Michael Wenzel¹ and Roland Mitric^{*1}

Institut für Physikalische und Theoretische Chemie, Universität Würzburg, Emil-Fischer Str. 42, 97074 Würzburg, Germany

(*Electronic mail: roland.mitric@uni-wuerzburg.de)

(Dated: 15 December 2022)

The theoretical prediction of the rates of nonradiative processes in molecules is fundamental to assess their emissive properties. In this context, global harmonic models have been widely used to simulate vibronic spectra as well as internal conversion rates and to predict photoluminescence quantum yields. However, these simplified models suffer from the limitations that are inherent to the harmonic approximation and can have a severe effect on the calculated internal conversion rates. Therefore, the development of more accurate semiclassical methods is highly desirable. Here, we introduce a procedure for the calculation of nonradiative rates in the framework of the time-dependent semiclassical Extended Thawed Gaussian Approximation (ETGA). We systematically investigate the performance of the ETGA method by comparing it to the the adiabatic and vertical harmonic method, which belong to the class of widely used global harmonic models. Its performance is tested in potentials that cannot be treated adequately by global harmonic models, beginning with Morse potentials of varying anharmonicity followed by a double well potential. The calculated radiative and nonradiative internal conversion rates are compared to reference values based on exact quantum dynamics. We find that the ETGA has the capability to predict internal conversion rates in anharmonic systems with an appreciable energy gap, whereas the global harmonic models prove to be insufficient.

I. INTRODUCTION

The efficiency of light-emitting molecular materials depends on the interplay between the radiative and nonradiative relaxation processes such as internal conversion (IC) and intersystem crossing (ISC) that compete with the emission of photons and can be detrimental to technological applications. For example, the function of light-emitting diodes (LEDs) in displays as well as fluorescence markers used as sensors in chemical or biological systems depend on efficient luminescence.^{1–8} Theoretical methods can directly contribute to technological advancement by virtual pre-screening of potential molecules, according to their properties like emission wavelength and fluorescence quantum yield. This requires efficient methods for the simulation of absorption and emission spectra as well as for predicting the rates of radiative and nonradiative relaxation processes. In this context, the prediction of the internal conversion rates is particularly challenging since the IC process can take place on an ultrafast timescale if the molecular system has accessible conical intersections connecting electronic states. This often leads to complex dynamics involving an intricate interplay of electronic and nuclear degrees of freedom. A proper treatment of such nonadiabatic dynamics requires methods that go beyond the Born-Oppenheimer approximation. A fully quantum mechanical treatment is possible using linear vibronic coupling models combined with the multilayer multiconfigurational time-dependent Hartree method (ML-MCTDH).^{9,10} While computationally demanding, this approach can handle strongly coupled electronic states and reveal their short time dynamics.¹¹ A second promising approach is the time-dependent density matrix renormalization group method (TD-DMRG).^{12–14}

An attractive alternative to these exact approaches are mixed quantum-classical methods using classical trajectories

that are allowed to hop between adiabatic electronic states, feasible even in systems that are too costly for a full quantum mechanical treatment.^{15–22}

The nonradiative decay of excited states can be slowed down by energetic barriers. In these cases the access to the conical intersection is the rate-determining step and can be treated using Kramers reaction rate theory.^{23–27} It is also possible that systems do not relax through a conical intersection but simply due to small, almost constant kinetic couplings. In this case, the nonradiative relaxation can be modelled within the time-dependent perturbation theory e.g employing Fermi's golden rule. Since systems in this limit are expected to show non-negligible fluorescence that is not suppressed by an ultrafast nonradiative decay, it would be desirable to have a theoretical approach for predicting the fluorescence quantum yields that relies on the perturbation theory but is more accurate than the widely used global harmonic models.^{28–35} The expressions for the internal conversion rate within the perturbation theory framework are based on Fermi's golden rule^{36,37} and existing methods differ in their approach and the approximations made to evaluate it. The prominent examples are the analytic energy gap law and its more recent variants that are applicable even to large molecular systems.^{24,38–43}

Another approach is to evaluate the sum-over-states rate expressions within a global harmonic approximation for the involved electronic potential energy surfaces.^{31,44,45} All required matrix elements are then available as analytic expressions but the quickly growing number of terms due to the high amount of possible vibronic transitions can make the summation cumbersome. A time-domain approach eliminates the need to evaluate the summation of matrix elements and replaces the problem with the task of propagating a nuclear wave packet to obtain an autocorrelation function. Analytic expressions for this autocorrelation function are also available within the global harmonic approximation.^{46–49}

However, the internal conversion usually occurs from a low lying vibrational state of the initial potential energy surface to a highly excited vibrational state of the final electronic potential. The prediction of the internal conversion rate may thus require an accurate treatment of higher lying vibrational states, which is not possible without an adequate handling of the anharmonicities of the underlying potential, which are completely absent in global harmonic models.⁵⁰ An attractive possibility to tackle this problem is provided by the various semi-classical methods for wave packet propagation.^{51–61} The basic idea is to express the initial state as a sum of Gaussian wave packets that are guided by classical trajectories, acquiring a phase factor according to the corresponding classical action. Differences exist in the details of the parametrization of the used Gaussian functions. They can be allowed to vary in width or remain frozen during the propagation.^{55,60} A major benefit is that only local information of the potential is required. Thus, it is not necessary to precompute the potential energy surface as is the case for quantum dynamics simulations. It was shown that this approach is applicable to the calculation of internal conversion rates in anharmonic potentials, using a semi-classical initial value representation method based on swarms of Gaussian wave packets.^{50,62} This approach can be used to model the dynamics of initial wave packets of arbitrary shape but may require many trajectories to converge.

In this work we introduce a method for the calculation of the internal conversion rates in the frame of the Extended Thawed Gaussian Ansatz (ETGA) that was recently used in a series of publications to predict vibronically resolved spectra.^{63–68} In this approach, the anharmonicity of a potential is automatically imprinted into the guiding trajectory and impacts the wave packet dynamics, which enables the method to treat cases where global harmonic models reach their limit. We explore the viability of the ETGA as tool for the prediction of radiative and nonradiative quantum yields in one-dimensional model systems that can be treated by exact numerical calculations. Furthermore, we compare systematically the performance of the ETGA with the global harmonic models. We begin by exploring the capabilities and limits of the ETGA model using Morse potentials with varying degrees of anharmonicity. This is followed by an application of the method to a double well potential with varying starting positions of the wave packet. We wish to emphasize that although one dimensional models are certainly not representative for complex polyatomic molecules the differences between approximations for calculation of rates are most clearly seen in one dimension, where exact results can be easily obtained.

II. THEORY

The ETGA method is derived by making the following ansatz for the time-dependent nuclear wave packet,⁶⁹

$$\phi_t(q) = \exp\left(i\left[\frac{1}{2}(q-q_t)^T A_t(q-q_t) + p_t^T(q-q_t) + \gamma_t\right]\right), \quad (1)$$

where all quantities are given in mass-weighted normal coordinates and Hartree atomic units. The time dependence is incorporated in the parameters A_t, q_t, p_t and γ_t , which satisfy the following differential equations

$$\dot{q}_t = p_t \quad \dot{p}_t = -V_t' \quad (2)$$

$$\dot{A}_t = -A_t A_t - V_t'' \quad (3)$$

$$\dot{\gamma}_t = i\frac{1}{2}\text{Tr}(A_t) + L_t, \quad (4)$$

that can be derived by inserting the wave packet ansatz into the time-dependent Schrödinger equation with a modified potential.⁵² The original potential is replaced by a time-dependent local harmonic approximation of the form

$$V_t(q) = V(q_t) + V_t'(q-q_t) + \frac{1}{2}(q-q_t)^T V_t''(q-q_t). \quad (5)$$

Solving differential equations (2–4) is equivalent to the propagation of a Gaussian wave packet using an effective time-dependent Hamiltonian⁵³

$$H_t = -\frac{1}{2}\nabla_q^2 + V_t(q) \quad (6)$$

such that

$$U\phi_0 = \phi_t, \quad (7)$$

with $U = \mathcal{T} \exp(-i \int_0^t H_t dt')$, introducing the time ordering operator \mathcal{T} . Since the parameters of the local harmonic potential are all time-dependent, such evolving potential can in principle accurately approximate any globally anharmonic potential energy surface. We will assume in the following that the initial state has a Gaussian shape, which is a good approximation for the vibrational groundstate of a system in equilibrium. A single Gaussian function with time-dependent parameters will then suffice, requiring only a single trajectory to be run. The parameters q_0, p_0, A_0 and γ_0 are determined by comparison with the initial vibrational ground state wave function.

The mass-weighted normal coordinate q_t and normal momentum p_t follow the classical equations of motion (2) and are obtained by running a classical trajectory on the original fully anharmonic adiabatic potential energy surface $V(q)$. This requires evaluations of the gradient $(V_t')_i = \frac{\partial V(q_t)}{\partial q_i}$, while the integration of equation (3) for A_t necessitates the calculation of the Hessian matrix $(V_t'')_{i,j} = \frac{\partial^2 V(q_t)}{\partial q_i \partial q_j}$. Parameter γ_t contains a classical contribution based on the Lagrangian $L_t = \frac{1}{2}p_t \cdot p_t - V_t$ evaluated along the trajectory q_t and ensures that the wave packet remains normalized.

The internal conversion rate will be calculated with the assumption that our system is initially in the vibrational ground state ϕ_{i0} of an adiabatic electronic excited state $|i\rangle$, which is assumed to be harmonic, close to its equilibrium configuration. The kinetic energy operator for nuclei, \hat{T} , is treated like a constant perturbation, facilitating a radiationless de-excitation to excited vibrational states of the adiabatic electronic ground

state. We consider all transitions from a single initial vibronic state ϕ_{i0} to the set of vibronic eigenstates $\{\phi_{fj}\}$ of the final potential energy surface, where the first and second indices indicate the electronic and vibrational state, respectively.

The transition rate according to Fermi's golden rule^{50,62,70} is given by

$$k_{\text{IC}} = 2\pi \sum_j |\langle \phi_{fj} | T_{fi} | \phi_{i0} \rangle|^2 \delta(\omega_{i0} - \omega_{fj}). \quad (8)$$

We switch to the equivalent time-dependent picture⁷¹ by introducing the Fourier integral representation of the Dirac delta distribution $\delta(\omega) = \frac{1}{2\pi} \int_{-\infty}^{\infty} dt \exp(i\omega t)$ into Eq. (8),

$$k_{\text{IC}} = \int_{-\infty}^{\infty} dt \exp(i\omega_{i0}t) \langle \phi_{i0} | T_{fi}^\dagger \sum_j |\phi_{fj}\rangle \exp(-i\omega_{fj}t) \langle \phi_{fj} | T_{fi} | \phi_{i0} \rangle. \quad (9)$$

Noticing that $\exp(i\omega_{i0}t) \langle \phi_{i0} | = \langle \phi_{i0} | U_i^\dagger$ and using the spectral representation of the propagator associated with the final electronic state, $U_f = \sum_j \exp(-i\omega_{fj}t) |\phi_{fj}\rangle \langle \phi_{fj}|$, leads to the following expression for the internal conversion rate

$$k_{\text{IC}} = \int_{-\infty}^{\infty} dt \langle \phi_{i0} | U_i^\dagger T_{fi}^\dagger U_f T_{fi} | \phi_{i0} \rangle. \quad (10)$$

The matrix element T_{fi} of the nuclear kinetic energy operator $\hat{T} = -\frac{1}{2} \nabla_q^2$ with respect to an orthogonal adiabatic electronic basis in mass-weighted normal coordinates is given by

$$T_{fi} = \langle f | \hat{T} | i \rangle_r = -\langle f | \nabla_q i \rangle_r^T \nabla_q - \frac{1}{2} \langle f | \nabla_q^2 i \rangle_r \quad (11)$$

We assume that the second-order nonadiabatic coupling $\langle f | \nabla_q^2 i \rangle_r$ can be neglected and use a constant value for the first-order nonadiabatic coupling $\tau_{fi} = \langle f | \nabla_q i \rangle_r$. This simplifies the kinetic coupling to the following expression

$$T_{fi} = -\tau_{fi}^T \nabla_q. \quad (12)$$

We will now focus on the core of the problem, that is the evaluation of the term

$$U_f | T_{fi} \phi_{i0} \rangle \quad (13)$$

which, besides some constant factors, is identical to the task of propagating the gradient of the initial thawed Gaussian. The gradient of Eq. (1) is readily evaluated and leads to

$$\nabla_q \phi_{i0} = (iA_0(q - q_0) + ip_0) \phi_{i0}. \quad (14)$$

The time evolution operator U_f does not commute with q . But it can be shown that it commutes with the initial momentum derivative operator ∇_{p_0} within the local harmonic approximation for the potential.⁶⁴ We can make use of this fact to rewrite Eq. (14) using the gradient with respect to the initial momentum

$$\nabla_q \phi_{i0} = (A_0 \nabla_{p_0} + ip_0) \phi_{i0}. \quad (15)$$

The propagator can now act directly on the initial wave packet,

$$\begin{aligned} U_f(t) \nabla_q \phi_{i0}(t_0) &= U_f(t) (A_0 \nabla_{p_0} + ip_0) \phi_{i0}(t_0) \\ &= (A_0 \nabla_{p_0} + ip_0) U_f(t) \phi_{i0}(t_0) \\ &= (A_0 \nabla_{p_0} + ip_0) \phi_{i0}(t). \end{aligned} \quad (16)$$

The time evolution of the wave packet is thus obtained by integration of the parameters that have been defined in Eqs. (2)–(4). The only additional step required is the evaluation of the gradient with respect to the initial momentum, which, as derived in Appendix D of reference 64, yields the following result

$$\nabla_{p_0} \phi_{i0}(t) = i(M_{t,pp}^T - M_{t,qp}^T A_t)(q - q_t) \phi_{i0}(t), \quad (17)$$

where we have introduced elements of the monodromy matrix M_t defined by

$$M_t = \begin{pmatrix} M_{qq} & M_{qp} \\ M_{pq} & M_{pp} \end{pmatrix} = \begin{pmatrix} \frac{\partial q_t}{\partial q_0} & \frac{\partial q_t}{\partial p_0} \\ \frac{\partial p_t}{\partial q_0} & \frac{\partial p_t}{\partial p_0} \end{pmatrix}, \quad (18)$$

with $\left(\frac{\partial q_t}{\partial q_0}\right)_{i,j} = \frac{\partial q_i(t, q_0, p_0)}{\partial q_{0,j}}$. The matrix is obtained by integration of the following equation^{72,73}:

$$\dot{M}_t = \begin{pmatrix} 0 & 1 \\ -V_t'' & 0 \end{pmatrix} M_t. \quad (19)$$

Assuming that internal conversion is the only competing decay channel allows the calculation of the quantum yield of spontaneous emission Φ as

$$\Phi = \frac{k_{\text{SE}}}{k_{\text{SE}} + k_{\text{IC}}}, \quad (20)$$

where the spontaneous emission rate k_{SE} is obtained by integration of the emission spectrum σ_{SE} ,^{45,65}

$$k_{\text{SE}} = \int_0^\infty d\omega \sigma_{\text{SE}} \quad (21)$$

with

$$\sigma_{\text{SE}}(\omega) = \frac{\omega^3}{6\pi^2 \hbar \epsilon_0 c^3} \int_{-\infty}^{\infty} dt \langle \phi_{i0} | U_i^\dagger \mu_{fi}^\dagger U_f \mu_{fi} | \phi_{i0} \rangle \exp(-i\omega t). \quad (22)$$

The transition dipole moment is defined as $\mu_{fi}(q) \equiv \mu_0 + \mu'(q - q_0)$, including the Franck-Condon and Herzberg-Teller term.⁷⁴⁻⁷⁶

Furthermore we will use the internal conversion correlation function from Eq. (10)

$$C(t) = \langle \phi_{i0} | U_i^\dagger T_{fi}^\dagger U_f T_{fi} | \phi_{i0} \rangle \quad (23)$$

to define $k_{\text{IC}}(\omega)$, the internal conversion spectrum

$$k_{\text{IC}}(\omega) = \int_{-\infty}^{\infty} dt C(t) \exp(i\omega t). \quad (24)$$

The angular frequency ω can be interpreted as the energy gap between the initial and final state and the internal conversion rate is contained in this spectrum at the point of energy conservation, $\hbar\omega = 0$ eV. Plots of the internal conversion rate as a spectrum show how the rate would change with the energy gap of the initial and final potential and peaks appear when $\hbar\omega$ matches the energy difference between states of the final and initial potential. Peaks at negative frequencies indicate states that are lower in energy than the initial state and those at positive energy correspond to higher lying states. This spectrum unveils all the information that is stored in the time-dependent correlation function and provides more information than the single valued rate by itself. It also constitutes a better measure to gauge and compare the quality of different methods.

III. MORSE POTENTIAL

A. Internal Conversion

The ETGA is exact for harmonic potentials since the local harmonic expansion is identical to the true potential in that case. A potential with anharmonicity is thus required to test the performance of the ETGA, with the Morse potential being ideally suited as its anharmonicity can be varied continuously.^{70,77} The results of the ETGA are compared to the results obtained using a split-operator propagation scheme^{78–81} (SOP) with the true potential as well as to the adiabatic and vertical harmonic approximations^{28,29,34} (AH and VH) in three Morse potentials with increasing anharmonicity. The initial potential is always the same and assumed to be harmonic and written in the form

$$V_i(q) = \frac{1}{2}\omega^2(q - q_{i,0})^2 + V_{i,0}, \quad (25)$$

the final potential is defined as

$$V_f(q) = D \left(1 - e^{-\frac{\omega}{\sqrt{2D}}(q - q_{f,0})} \right)^2 + V_{f,0}. \quad (26)$$

The anharmonicity of the Morse potential⁷⁰ is defined as

$$\chi = \frac{\omega}{4D}. \quad (27)$$

The fundamental frequency is the same for the initial and final potential and is kept constant at $\omega = 3000 \text{ cm}^{-1}$. The minima of the potentials are $30 m_e^{1/2} a_0$ mass weighted units apart. The first order kinetic coupling parameter is in all cases $\tau_{fi} = 1.0 (m_e^{1/2} a_0)^{-1}$. The adiabatic energy difference of the potentials is set constant at 3.0 eV. We begin with an anharmonicity of $\chi = 0.002$ corresponding to a well depth $D = 46.5 \text{ eV}$. The initial harmonic potential and the Morse potential are shown in Figure 1, together with the vertical and adiabatic harmonic approximations to the final potential. The initial potentials in our models are always assumed to be a harmonic approximation to an adiabatic electronic potential and as such may cross the final potential while working in an adiabatic basis with derivative couplings. The turning points

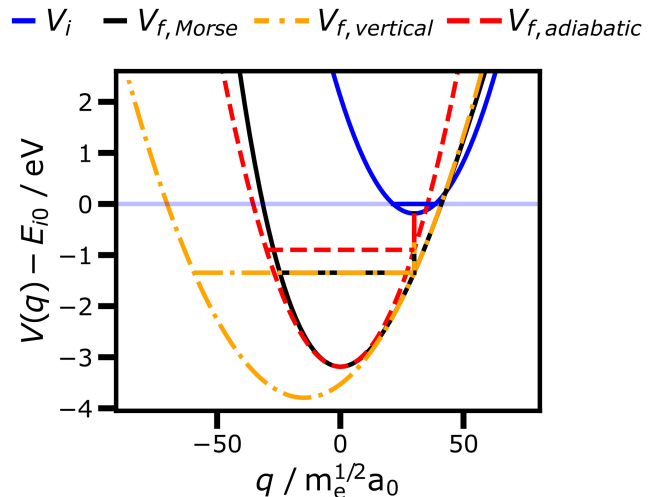


FIG. 1. Initial (blue) and final (black) potential, together with the vertical (orange) and adiabatic (red) harmonic approximation to the final potential. The final potential is a Morse potential with anharmonicity $\chi = 0.002$. The energy axis is shifted by E_{i0} , the eigenvalue of the initial vibrational eigenstate of harmonic potential V_i . Horizontal lines in the same color and linestyle as the potentials indicate the starting and turning points of classical trajectories that start at the equilibrium position of V_i .

of a classical trajectory starting at the equilibrium position of the initial potential are indicated by horizontal lines.

The difference between the vertical and adiabatic approximation is clearly visible even in the case of low anharmonicity and it is a priori not certain which of the harmonic approximations is better suited for the calculation of nonadiabatic transition rates. The VH model is able to capture the short-time dynamics more accurately than the AH model, but at the same time the vertical model should have a larger error regarding wave packet recurrence times, which determine the splitting⁵⁴ of individual vibrational states. The one dimensional model allows a convenient visualization of the wave packet dynamics as shown in Figure 2. The center of the wave packet follows closely the classical trajectory (indicated by orange squares), even when using a full quantum mechanical treatment (Fig. 2a) without approximations as long as the anharmonicity is low. But the delocalisation and spreading of the wave packet clearly increase with each reflection at the turning point of the trajectory. These effects cannot be captured by a single Gaussian, even if its width is varying with time. The VH wavefunction (Fig. 2d) travels to regions that are energetically forbidden in the true Morse potential, while the AH (Fig. 2c) and ETGA wavefunction (Fig. 2b) appear quite similar to the propagation based on the original potential.

The corresponding autocorrelation functions are provided in Figure 3a–d. Time evolution under the true Morse potential leads to a spreading of the wavepacket and thus a decreasing overlap with the initial wavefunction which expresses itself as slow decay of the correlation function (Fig. 3a). The ETGA can reproduce this behavior (Fig. 3b) unlike the global harmonic models, where the magnitude of the overlap keeps

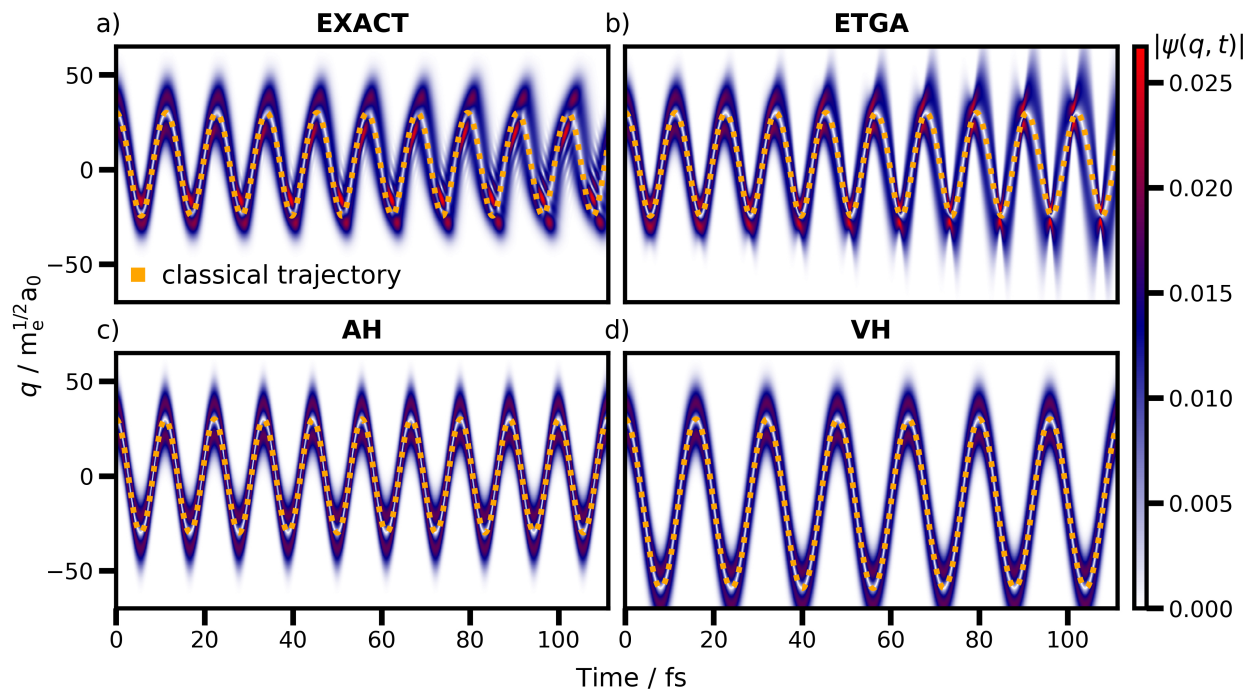


FIG. 2. Magnitude of the wavepacket $\psi(q, t) = \langle q | U_f T_{fi} | \phi_{i0} \rangle$ obtained by numerical propagation using a split-operator scheme (a), the extended thawed Gaussian Ansatz (b), the adiabatic harmonic approximation (c) and the vertical harmonic approximation (d). The final potential V_f is a Morse potential with an anharmonicity of 0.002.

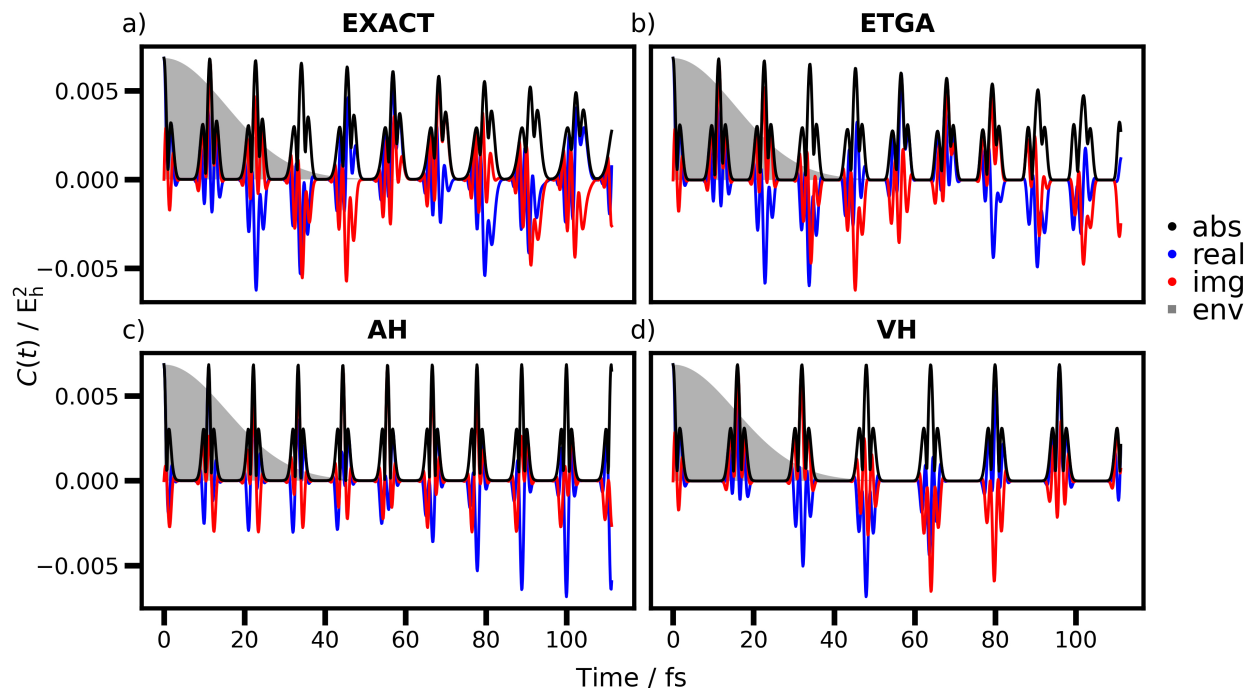


FIG. 3. Auto correlation function $C(t) = \langle \phi_{i0} | U_i^\dagger T_{fi}^\dagger U_f T_{fi} | \phi_{i0} \rangle$ obtained by numerical propagation using a split-operator scheme (a), the extended thawed Gaussian Ansatz (b), the adiabatic harmonic approximation (c) and the vertical harmonic approximation (d). The final potential V_f is a Morse potential with an anharmonicity of 0.002. The time-domain Gaussian envelope (env), corresponding to a HWHM of 0.05 eV in the frequency domain, is shown as grey background.

returning to its initial value (Fig. 3c,d). Extraction of the spectral content is provided using a Fourier transform. The correlation function is mirrored and conjugated to extend the signal to negative times. It is then weighted with a Gaussian lineshape function to remove Gibbs artifacts that would occur due to the sudden cutoff of the signal after the finite propagation time of $T = 10 \frac{2\pi}{\omega} \approx 111.2$ fs.

The spectrum based on the SOP propagation scheme serves as reference in the comparison of the different approximations and is labelled as EXACT in the figures. The top panel of Figure 4 shows the reference and the ETGA spectrum. The agreement is very good and the position and height of the peaks are well reproduced over the whole energy range. The adiabatic harmonic model (Fig. 4b) manages to describe the energetically low lying states but fails at higher energies. The vertical model (Fig. 4c) performs better in that region but shows shortcomings in the low energy region. The ETGA is in this case clearly superior to either of the global harmonic approximations.

The reliability of the ETGA was further tested by increasing the anharmonicity of the Morse potential from 0.002 to 0.004 and finally 0.008, moderate values that ensure that the second derivative of the Morse potential remains positive at the initial geometry, so that the vertical harmonic approximation to the potential remains bound. This corresponds to decreasing values of the well depth parameter D from 46.5 eV to 23.2 eV and lastly 11.6 eV. The spectra for the case with medium anharmonicity of 0.004 are shown in Figure 5a–c, the case with an anharmonicity of 0.008 in Figure 5d–f. Increasing the anharmonicity to 0.004 has little effect on the quality of the ETGA spectrum (Fig. 5a), it is still able to reproduce the exact spectrum remarkably well. But the limitations of the method begin to show in Figure 5d as the anharmonicity is further increased. Peaks with negative intensity begin to appear as a consequence of the time dependent nature of the approximation, as well as peaks that are nonexistent in the reference. The approximation still matches the reference spectrum to a good degree but it becomes clear that the reliability is diminishing. The adiabatic harmonic approximation is the same for all cases (Fig. 5b,e) as the second derivative at the minimum stays constant at $\omega = 3000$ cm⁻¹ for the Morse potentials. The spacing between consecutive states is constant, leading to an overestimation of the energy gap of excited states that are moving closer together in the true potential. The vertical harmonic approximation (Fig. 5c,f) has a similar problem. The second derivative evaluated at the starting position of the wave packet corresponds to angular frequencies that decrease as the anharmonicity of the Morse potential is increased. The vertical harmonic potentials take on values for ω of 2083, 1742, 1279 cm⁻¹ for the three anharmonicity parameters 0.002, 0.004, 0.008. This leads to an underestimation of the energy gap for low lying states of the potential and the states are bunching together in the energy range of interest.

The vertical harmonic model can capture the envelope of the vibronic pattern over the whole range of energies but agreement with the exact vibronic pattern cannot be achieved for any of these levels of anharmonicity. In contrast, the adiabatic harmonic model can be trusted for low lying vibrational

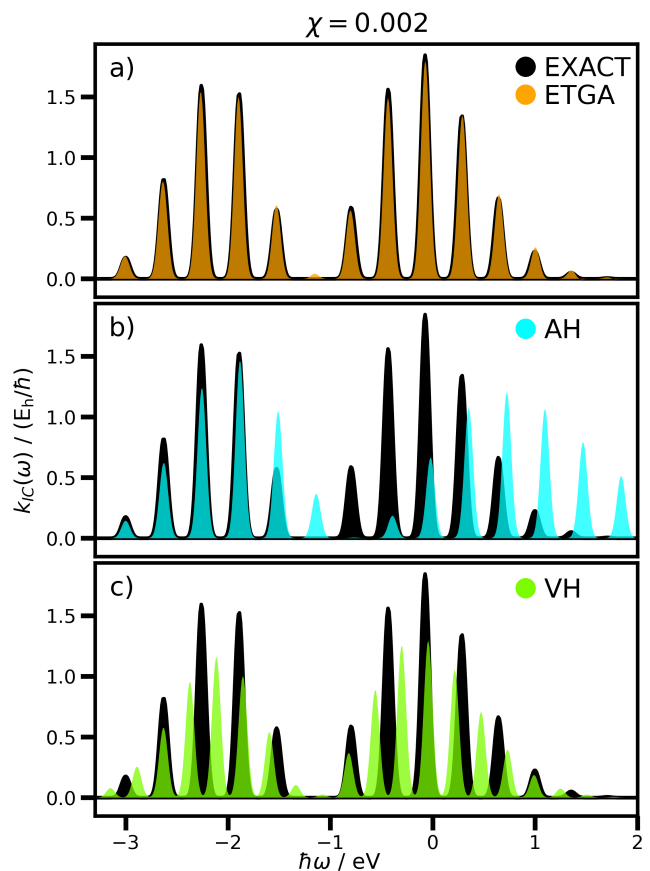


FIG. 4. Internal conversion spectrum (Eq. (24)) based on a Morse potential with anharmonicity of 0.002. The reference spectrum in black shows the results based on the Morse potential without approximations. The spectrum using the ETGA is given in orange in the top panel (a). The middle plot (b) shows the adiabatic harmonic approximation spectrum (cyan) and the bottom (c) the vertical harmonic approximation spectrum (green). The spectra are based on the correlation functions shown in Figure 3 and broadened with a Gaussian line shape function with a half width at half maximum (HWHM) of 0.05 eV. The internal conversion rate is the value of the spectrum at $\hbar\omega = 0$ eV. Spectra are not shifted or scaled to improve agreement with the reference.

states and might be suitable if the final and initial states are energetically very close, but its ability to capture the features of the spectrum worsens quickly for higher lying states. Even the general shape begins to deviate notably at higher energies. One can get either the envelope right by using the VH model or the transitions to the lowest vibrational states using the AH model. The extended thawed Gaussian Ansatz is a clear improvement and yields reasonable results at the whole range of energies, where the harmonic approximations begin to fail.

B. Spontaneous Emission

The numerical values of the transition dipole moment μ_0 and its derivative μ' are chosen for all calculations such that

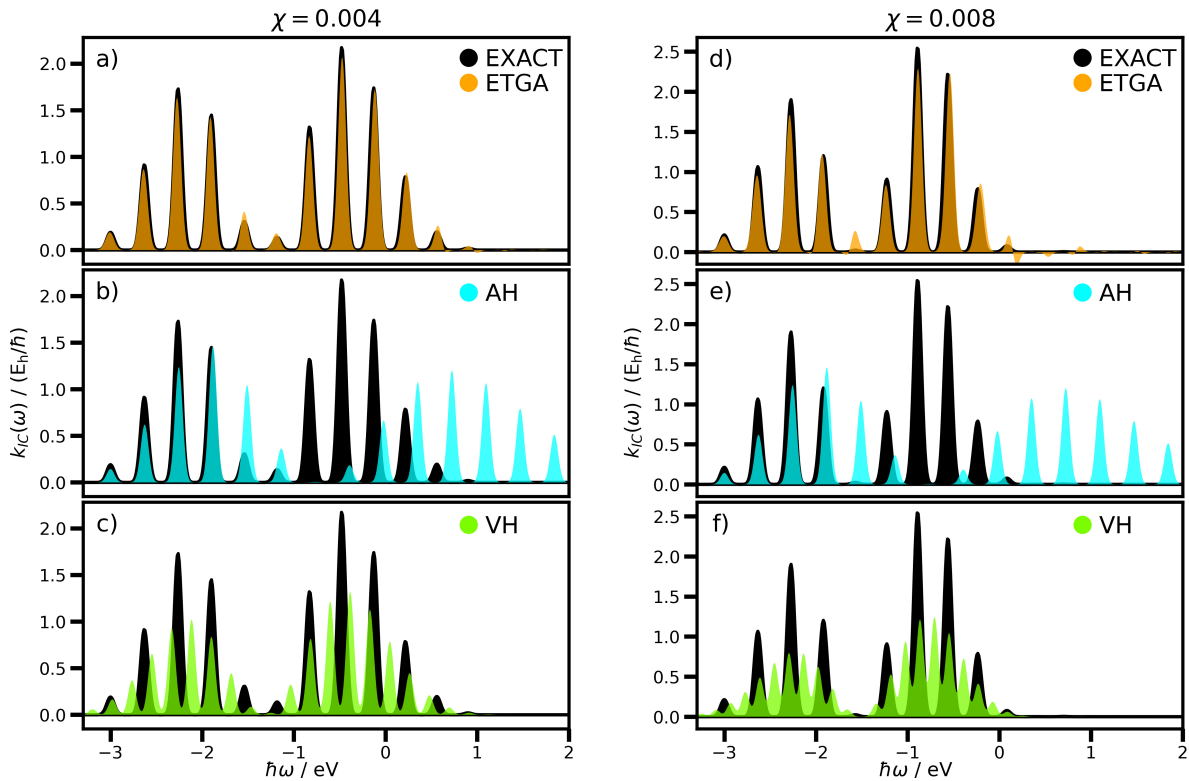


FIG. 5. Internal conversion spectra based on a Morse potential with anharmonicity of 0.004 (left column, a–c) and 0.008 (right column, d–f). The reference spectrum in black is based on the Morse potential without approximations. The top panels (a,d) show the ETGA spectrum in orange, the adiabatic harmonic model (cyan) is in the middle (b,e) and the vertical harmonic model (green) at the bottom (c,f). All spectra have been broadened using a Gaussian line shape function with a HWHM of 0.05 eV.

$\frac{\mu_0}{(6\pi^2\hbar\epsilon_0c^3)^{1/2}} = 10$ a.u. and $\frac{\mu'}{(6\pi^2\hbar\epsilon_0c^3)^{1/2}} = -0.5$ a.u. These values yield emission rates of similar magnitude to the internal conversion rates, which is necessary in order to obtain reasonable quantum yields. The emission spectra for the Morse potentials with low and high anharmonicity are given in Figures 6a–c and 6d–f, the intermediate case with anharmonicity $\chi = 0.004$ is not explicitly shown.

The 0-0 transition corresponds to the peak at 3.0 eV, while transitions to states with a higher vibrational quantum number are found to the left of it. The intensity of peaks corresponding to transitions to states with a small energy gap to the initial state, decreases and approaches zero as the gap closes due to the scaling of spontaneous emission with ω^3 . This scaling means that the prediction of states with a noticeable gap is more relevant when it comes to the prediction of emission rates, unlike internal conversion rates, where an accurate description of states with a vanishing energy gap is essential. We can observe that the ETGA (Fig. 6a,d) provides overall a good description of intensities and frequencies. The method however produces weak erroneous peaks at frequencies that are too high, wrongly implying the existence of states below the vibrational ground state of the final potential.

This problem is also observed in the vertical harmonic model (Fig. 6c,f), but unlike the ETGA, it shows poor performance predicting intensities and frequencies over the whole

range of transition frequencies. The adiabatic harmonic model (Fig. 6b,e) on the other hand gives reasonable results close to the 0-0 transition and benefits from the suppression of peaks at small energy gaps, which hides the shortcomings of the model in describing highly excited vibrational states. It also lacks the erroneous peaks at high transition energies but the intensities and the peak spacing are not as good as in the case of the ETGA model.

C. Quantum Yields

We can now proceed to the calculation of radiative quantum yields. Integration of the emission spectra yields the spontaneous emission rate, and the internal conversion rate is given by the value of the internal conversion spectrum evaluated at zero energy. The quantum yield is then obtained using Eq. (20), giving rise to the results summarized in Table I.

The ETGA is an improvement over the global harmonic models. The emission rates are in excellent agreement with the exact values, just like the emission spectra in Fig. 6a/d. The internal conversion rates are also in good agreement but the spectra (Fig. 5) also show the downside of using a time dependent ansatz. The ETGA does not guarantee positive valued spectra. This can be problematic for internal conversion rates, which are evaluated at a single frequency if we adhere strictly

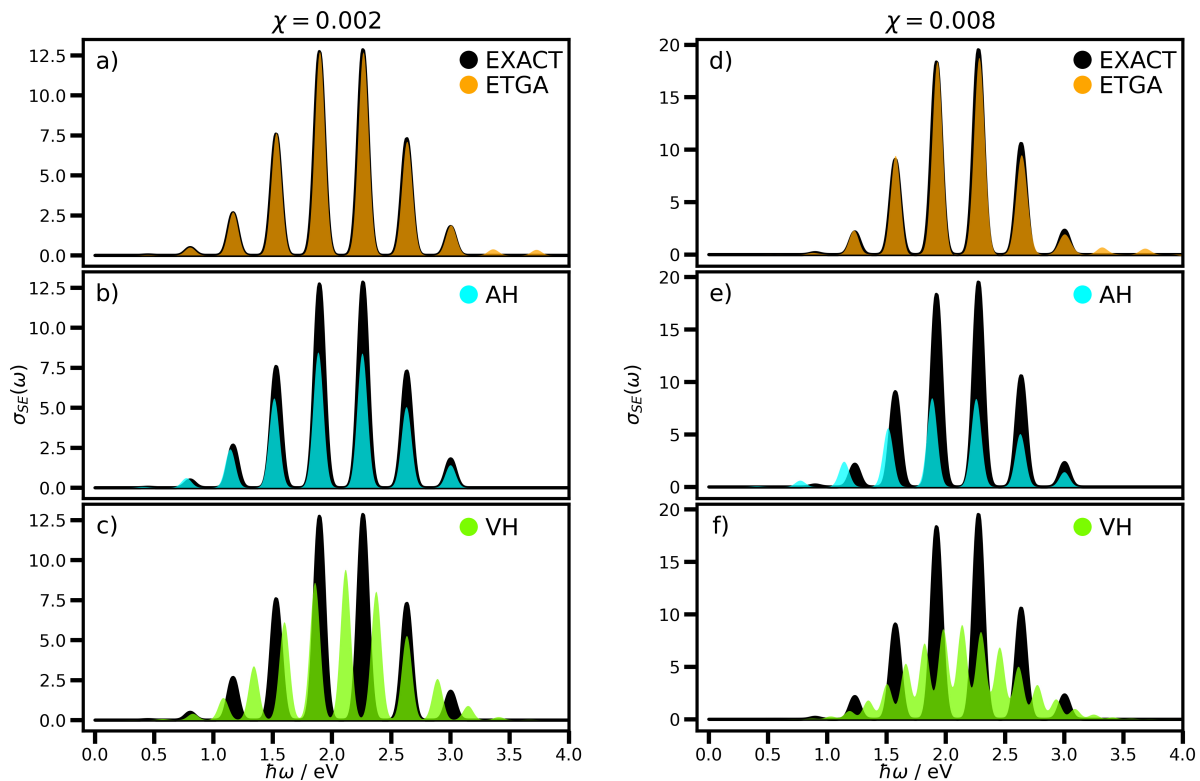


FIG. 6. Spontaneous emission spectrum based on a Morse potential with anharmonicity of 0.002 (left column, a–c) and anharmonicity 0.008 (right column, d–f). The reference spectrum in black is based on the Morse potential without approximations. The top panels (a,d) show the ETGA spectrum in orange, the adiabatic harmonic model (cyan) is in the middle (b,e) and the vertical harmonic model (green) at the bottom (c,f). All spectra have been broadened using a Gaussian line shape function with a HWHM of 0.05 eV. The corresponding emission rates are obtained by integration of the spectra.

TABLE I. Internal conversion rate, spontaneous emission rate and radiative quantum yield for varying degrees of anharmonicity χ of a Morse potential.

$\chi = 0.002$	EXACT	ETGA	AH	VH
$k_{IC}/(E_h/\hbar)$	3.94×10^{-1}	4.24×10^{-1}	5.93×10^{-1}	7.50×10^{-1}
$k_{SE}/(E_h/\hbar)$	1.78×10^{-1}	1.81×10^{-1}	1.25×10^{-1}	1.81×10^{-1}
$\Phi_{QY} \times 10^2$	31.1	29.9	17.4	19.5
$\chi = 0.004$	EXACT	ETGA	AH	VH
$k_{IC}/(E_h/\hbar)$	1.79×10^{-2}	4.40×10^{-2}	5.93×10^{-1}	4.31×10^{-1}
$k_{SE}/(E_h/\hbar)$	2.04×10^{-1}	2.08×10^{-1}	1.25×10^{-1}	2.08×10^{-1}
$\Phi_{QY} \times 10^2$	91.9	82.5	17.4	32.5
$\chi = 0.008$	EXACT	ETGA	AH	VH
$k_{IC}/(E_h/\hbar)$	1.19×10^{-2}	3.06×10^{-3}	5.93×10^{-1}	5.23×10^{-2}
$k_{SE}/(E_h/\hbar)$	2.44×10^{-1}	2.48×10^{-1}	1.25×10^{-1}	2.48×10^{-1}
$\Phi_{QY} \times 10^2$	95.3	98.8	17.4	82.6

to energy conservation. The method does deliver the best agreement if we judge the spectrum as a whole but it can give nonphysical results at specific energies. The method also suffers from decreasing accuracy as the anharmonicity increases. It does yield the best results however and the overall agreement of both spectra — emission and internal conversion—

allows for a higher degree of confidence than pure harmonic models, especially in the case of internal conversion where the anharmonicity of the potential needs to be taken into account.

The emission spectra based on the adiabatic harmonic approximation show notable deviations in the peak intensities as the anharmonicity increases, but the predicted frequencies are reasonable. The decrease of the dissociation energy that is used to raise the anharmonicity has no effect on the adiabatic approximation due to the constant second derivative at the equilibrium position. The AH model yields in all cases the same results, independent of the increasing anharmonicity. It is adequate for transitions to the first few vibrational states of the final potential, but the energy of higher lying states is overestimated. This leads to large deviations in the case of the internal conversion spectra, where the energy conserving transition ends in an highly excited vibrational state.

A quick glance at the quantum yields suggests that the VH model is superior to the AH model. The integrated areas of the emission spectra are close to the exact ones, due to the VH method's ability to capture the correct short-time dynamics, which determines the overall envelope and area. Due to this fact, the integrated emission rates are virtually identical to the results of the ETGA method, with the benefit of a much lower computational cost. But the internal conversion rate poses some difficulty. It is clear that the individual vibrational states

of the final potential are incorrect in the vertical model, which can cause deviations regarding the internal conversion rate. This is due to the fact that the IC rate is not obtained by integration but determined by the detailed shape of the spectrum at the point of energy conservation. The vibrational frequency for the vertical harmonic approximation is derived at a position where the Morse potential shows more gentle incline. As the anharmonicity increases, the frequencies decrease further and the energy gap between states gets underestimated, leading to spectra with closely spaced peaks which can lead to a coincidental intersection of the vertical harmonic and exact spectra at the relevant value. It is not possible to predict a priori whether the VH model matches the true value or not for the internal conversion rate as long as the vibronic states remain separated. The AH model on the other hand is correct for the first few vibrational states but most likely wrong if there is a notable energy gap between initial and final state.

IV. SYMMETRIC DOUBLE-WELL POTENTIAL

A. Internal Conversion and Emission Spectra

The ETGA was already applied to simulate wave packet dynamics on double-well potential energy surfaces of Pnictogen hydride cations to obtain vibronically resolved photoelectron spectra⁶⁸. It was shown that the quality of the results varies, depending on the width and initial position of the wave packet with respect to the double-well. The method is used here to predict internal conversion rates, to test its ability and reliability to handle floppy molecules when it comes to the estimation of quantum yields.

The final potential is assumed to be a symmetric double-well defined by

$$V_f(q) = \frac{b}{q_{f,0}^4} (q - q_{f,0})^2 (q + q_{f,0})^2 + V_{f,0} \quad (28)$$

The minima of the double well are at $q_{f,0} = \pm 145.747 m_e^{1/2} a_0$ and the energetic barrier between them is given by $b = 1.5$ eV. This choice of parameters leads to an angular frequency $\omega_f = 1000$ cm^{-1} in a harmonic approximation at $q_{f,0}$ for the adiabatic harmonic model. While the final potential remains the same, shifted harmonic potentials with angular frequency $\omega_i = 1500$ cm^{-1} and $V_0 = 3.0$ eV are used to define the initial wave packet. The setup consists of three cases, with $q_{0,A} = 190.428 m_e^{1/2} a_0$, $q_{0,B} = 210.206 m_e^{1/2} a_0$, and $q_{0,C} = 223.616 m_e^{1/2} a_0$. The initial positions were chosen based on the associated classical trajectories in the final double well potential. The classical energy for a trajectory starting at $q_{0,A}$ is 0.75 eV, half the value of the barrier, leading to a wave packet trapped to one side of the well. The energy at $q_{0,B}$ is slightly above the barrier with 1.75 eV and the last case with $q_{0,C}$ as initial position corresponds to an energy of 2.75 eV considerably above the barrier.

A second order Taylor expansion of the final potential for each initial position yields the harmonic potentials used in the

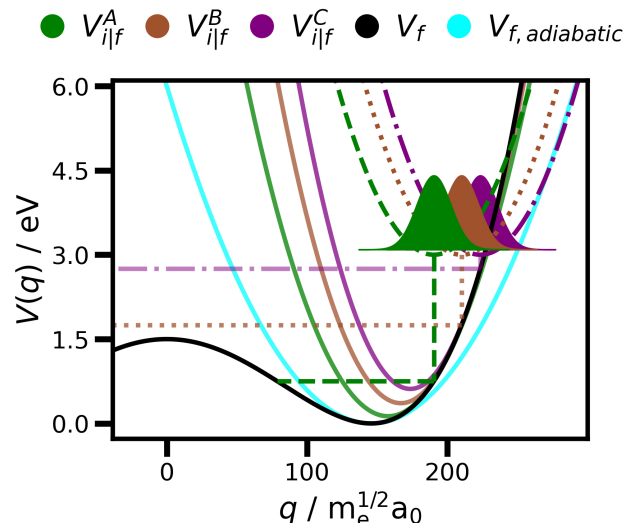


FIG. 7. Symmetric double well potential and three shifted harmonic potentials that are used for the simulation of internal conversion and spontaneous emission. The horizontal lines indicate the initial position and turning point of classical trajectory that start at the equilibrium positions of the initial harmonic potentials $V_{i|f}^A$, $V_{i|f}^B$, and $V_{i|f}^C$. The adiabatic harmonic approximation $V_{f,adiabatic}$ of the double well potential V_f is constructed by harmonic expansion around the closest minimum of the double well with respect to the initial potential minimum. The potentials for the vertical harmonic model are also shown and indicated as V_f^A , V_f^B and V_f^C .

vertical harmonic model. The frequencies of these harmonic oscillators are $\omega_A \approx 1435$ cm^{-1} , $\omega_B \approx 1619$ cm^{-1} and $\omega_C \approx 1741$ cm^{-1} . Figure 7 shows the potentials, the initial state wave function and the classical energy. The wave packets are again propagated using the exact potential in a split-operator scheme, the ETGA, the VH and the AH model. The transition dipole moment coupling parameters are $\frac{\mu_0}{(6\pi^2\hbar\epsilon_0 c^3)^{1/2}} = 10$ a.u. and $\frac{\mu'}{(6\pi^2\hbar\epsilon_0 c^3)^{1/2}} = -0.5$ a.u. The kinetic coupling for internal conversion is set to $\tau_{fi} = 1.0 (m_e^{1/2} a_0)^{-1}$. The wave packets were in all cases propagated for $T = 10\pi/\omega_f \approx 166$ femtoseconds to obtain the correlation functions.

In this case we also explore how the radiative and nonradiative rate vary as a function of the width of a Gaussian envelope, which determines the damping of the correlation function from a time-domain point of view. With this we can assess how the method performs as we look at the statistical limit for relaxation⁸²⁻⁸⁷, the case where the lifetime of the final states is short. This corresponds to the assumption that the relaxation of the final states is faster than the recurrence time of the wave packet which is assumed to be the case in large poly-atomic molecules or systems in contact with an environment. In either case one can assume that there is a high density of states that couple to the final vibronic states of the molecule, leading to a fast vibrational relaxation that limits the lifetime. This is in contrast to the former example of the Morse potential where we included recurrences of the wave packet and assumed a long lifetime of the final vibrational states. For our one-dimensional model we assume that the

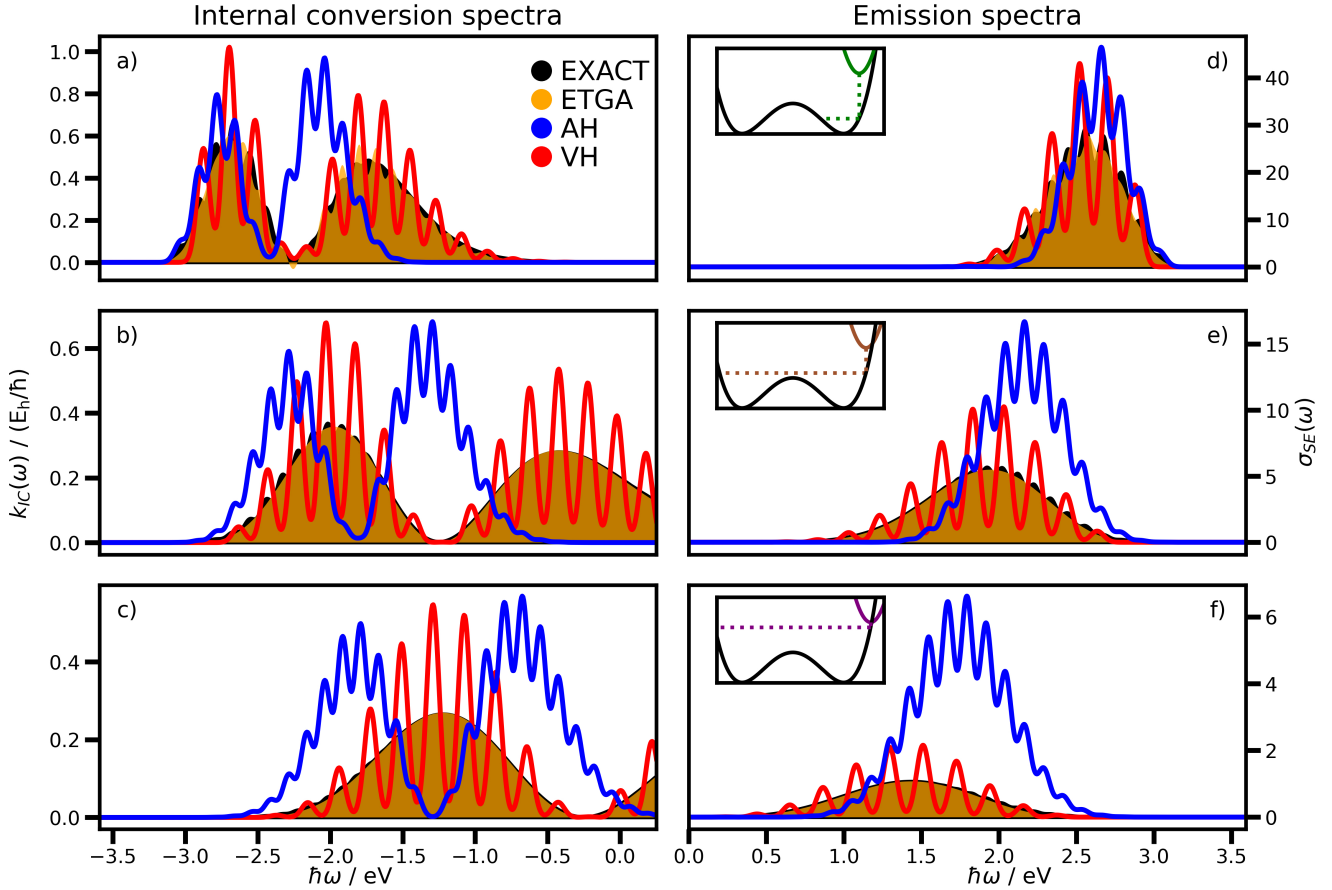


FIG. 8. Internal conversion (left column, a–c) and spontaneous emission (right column, d–f) spectra of a double well potential (Fig. 7). The position of the initial potential was chosen based on the potential energy of the classical trajectories in the double well. Position $q_{0,A}$ (a,d) leads to dynamics trapped to the initial side of the well, $q_{0,B}$ (b,e) and $q_{0,C}$ (c,f) corresponds to a trajectories with enough potential energy to cross the barrier as shown in the insets in the emission spectra. The reference spectra based on the exact potential are shown in black (filled), the ETGA results are given in orange (filled), the adiabatic harmonic model was used to obtain the blue-colored (line) spectra and the vertical harmonic model results are given in red. The internal conversion rates are given by the values of the IC spectra at $\hbar\omega = 0$ eV, while the radiative rates are obtained by integration of the emission spectra. All spectra were broadened with a Gaussian line shape function with a HWHM of 0.05 eV.

broadening is due to an environment and use thus a Gaussian line shape. We begin with a small spectral width of 0.05 eV for the Gaussian HWHM to see the vibronic structure due to individual states. The results for internal conversion and emission are shown shown in Figure 8 side by side.

The internal conversion spectra given in Figure 8a are based on the trapped wave packet. The internal conversion rate is the value of the spectrum at energy conservation, i.e. an energy difference of final and initial state of zero. The rate value is negligible in this case but the internal conversion spectrum shows that the ETGA (orange filled) provides a better approximation to the exact reference spectrum (black filled) as the energy gap closes while the adiabatic harmonic approximation (blue line) is better suited to model the transition to the vibrational ground state of the final potential. The vibronic structure of the vertical harmonic model is quite pronounced but does not match the real states, however the general shape is in fair agreement and does not deviate as strongly as the

adiabatic model as the energy increases. The corresponding emission spectra are given in Figure 8d. The adiabatic harmonic approximation spectrum seems to be superior to the ETGA in the prediction of the 0-0 transition at 3.031 eV but starts to overestimate the intensities for transitions to higher vibrational states compared to the exact reference spectrum. The ETGA spectrum however yields decent results as the energy gap between final and initial states grows smaller.

Figures 8e,f depict the emission spectra of wave packets that can cross the barrier. The ETGA emission spectra are lacking any separation of vibronic states, but the general shape and intensities are close to the exact result in both cases. The explanation for this is the ETGA's ability to capture the initial, short-time wave packet dynamics. This yields good results for the central frequencies and envelopes of the observed peak patterns, but a prediction of the fine splitting requires a good description for a longer duration, when the thawed Gaussian approximation for the wave packet would fall off in quality

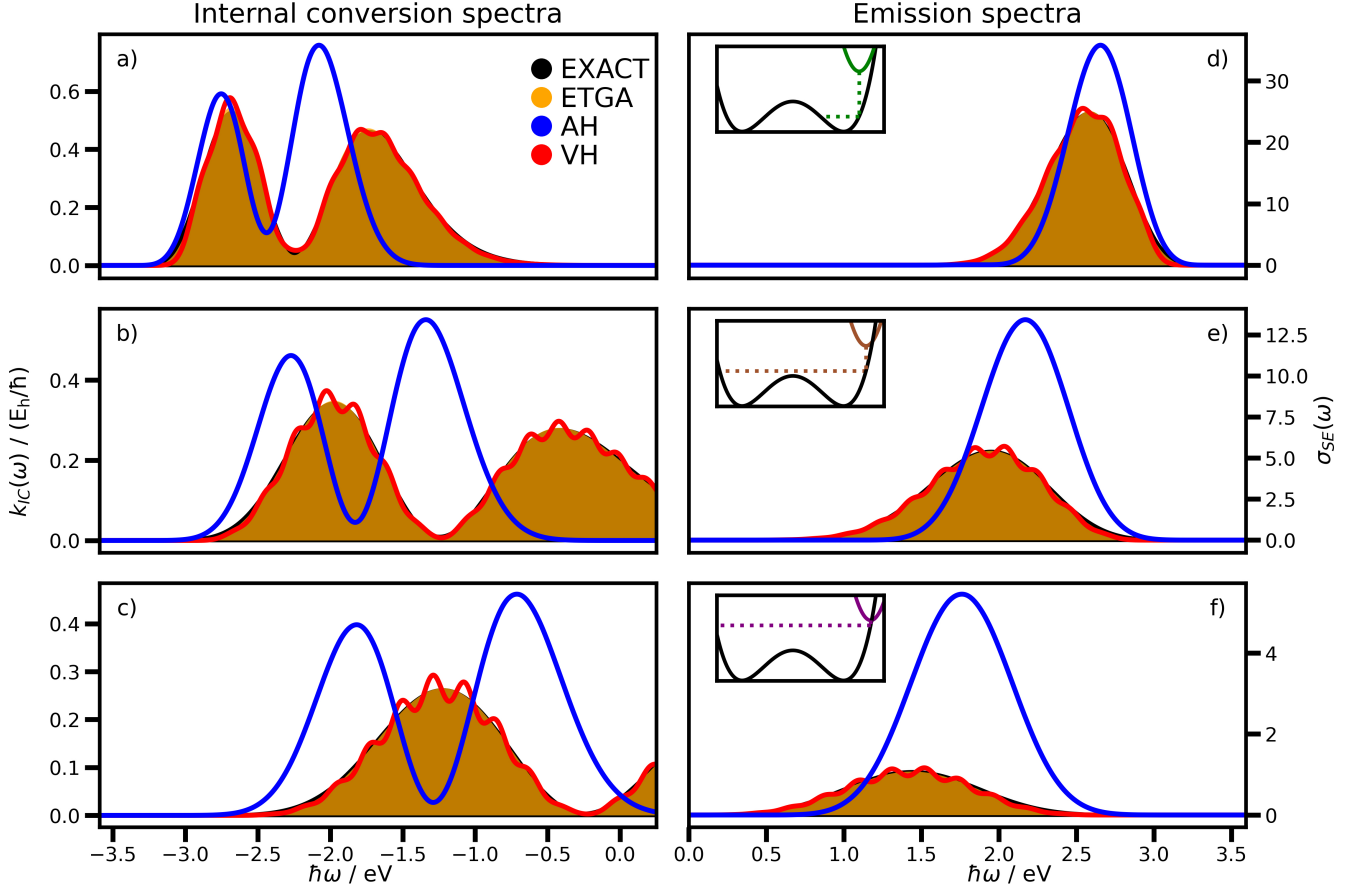


FIG. 9. Internal conversion (left column, a–c) and spontaneous emission (right column, d–f) spectra of a double well potential (Fig. 7). The position of the initial potential was chosen based on the potential energy of the classical trajectories in the double well. Position $q_{0,A}$ (a,d) leads to dynamics trapped to the initial side of the well, $q_{0,B}$ (b,e) and $q_{0,C}$ (c,f) corresponds to a trajectories with enough potential energy to cross the barrier as shown in the insets in the emission spectra. The reference spectra based on the exact potential are shown in black (filled), the ETGA results are given in orange (filled), the adiabatic harmonic model was used to obtain the blue-colored (line) spectra and the vertical harmonic model results are given in red. The internal conversion rates are given by the values of the IC spectra at $\hbar\omega = 0$ eV, while the radiative rates are obtained by integration of the emission spectra. All spectra were broadened with a Gaussian line shape function with a HWHM of 0.1 eV.

with time. The adiabatic approximation largely overestimates the intensities and the constant peak spacing of the harmonic model leads to growing errors in the frequency for transitions to higher lying vibrational states of the double well potential. This is especially problematic for the internal conversion rate, seen in Figures 8b,c. Here, the general shape of the adiabatic model is a poor fit to the reference. The curve of the adiabatic harmonic model crosses the reference spectrum at some points, but the agreement of the values is clearly accidental and not systematic nor reliable, barring the 0-0 transition. The vertical harmonic model is also superior to the adiabatic approximation although the pronounced vibronic structure is clearly undesirable in this case, as it predicts noticeable fluctuations in the internal conversion rate with small energy shifts.

We proceed by increasing the HWHM of the spectral envelope from the former 0.05 eV to 0.1 eV, corresponding to a damping of the correlation function such that recurrences are almost suppressed. In this case the spectrum is determined by

the initial decay of the correlation function, given by the time the wave packet needs to leave the region of overlap initially. The results are gathered in Figure 9. Individual peaks can no longer be distinguished as the vibronic structure is smoothed out. The splitting due to recurrences in the correlation function is gone and the form of the spectrum is dominated by the envelope due to the fast initial decay time. The ETGA and vertical harmonic model yield almost the same results and it becomes clear that they will converge for even higher values of the HWHM. The time-dependent potential used in the ETGA is approximately constant on this short timescale and at the start of the dynamics it is identical to the potential used in the vertical harmonic model. There clearly is a time-scale on which both models are barely distinguishable and the models will converge to the same results if the initial decay occurs on this time-scale. The adiabatic harmonic model is inferior since it is generally not the best harmonic approximation to the true potential around the point where the initial dynamics takes place; barring the case where the initial and final equilib-

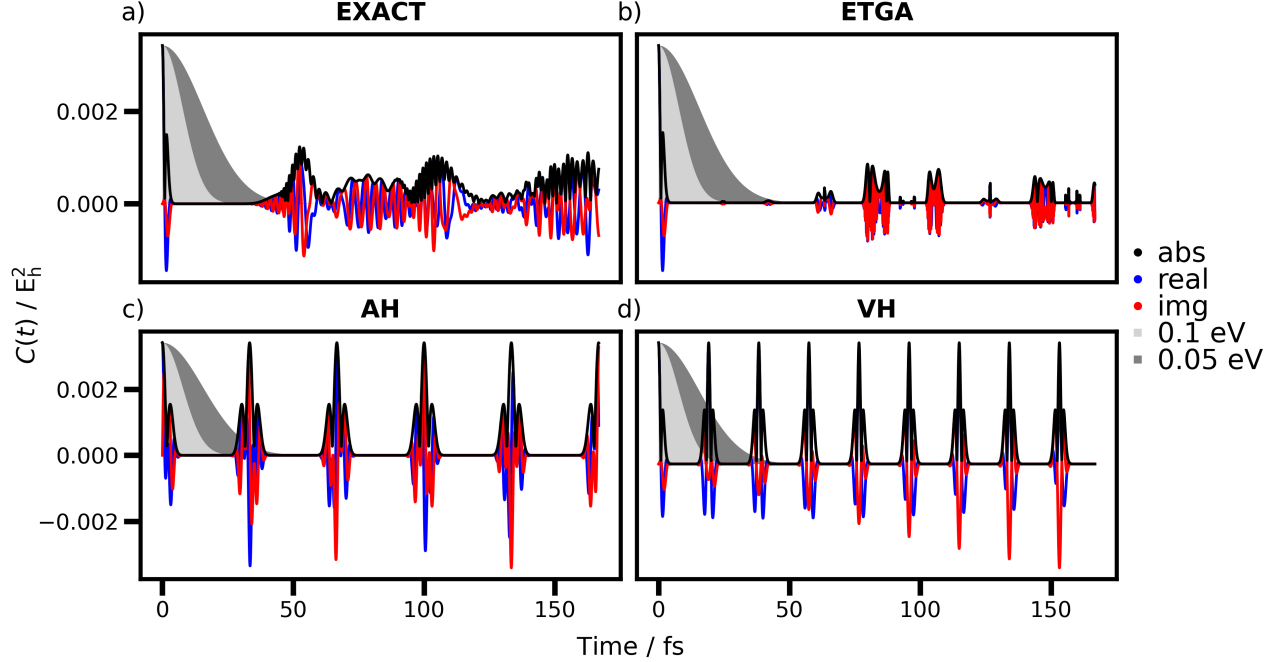


FIG. 10. Auto correlation function $C(t) = \langle \phi_{i0} | U_i^\dagger T_{fi}^\dagger U_f T_{fi} | \phi_{i0} \rangle$ obtained by (a) numerical propagation using a split-operator scheme, (b) the extended thawed Gaussian Ansatz, (c) the adiabatic harmonic approximation and (d) the vertical harmonic approximation for the transition from V_i^C to the double well potential as shown in Figure 7. The time-domain Gaussian envelopes, corresponding to a HWHM of 0.1 eV and 0.05 eV in the frequency domain, are shown in light gray and gray as background.

rium position are identical. The time scale is easily identified in Figure 10, showing the internal conversion correlation function for initial potential C. There are no simple recurrences in the exact correlation function (Fig. 10a) as the wave packet dynamics is quite complicated and far from the harmonic case. The time-domain correlation function (Fig. 10b) also shows that the ETGA method is not able to capture the long-term dynamics correctly in this case, meaning that it could not resolve the vibronic structure even if we had chosen a very small spectral line width. The time for the initial decay is clearly overestimated in the AH model (Fig. 10c), explaining its failure to predict the envelopes of the spectra. The VH model (Fig. 10d) on the other hand shows good agreement on the shortest time scale, to which the dynamics is restricted when damped by the Gaussian corresponding to a spectral width of 0.1 eV. The HWHM value of 0.05 leads to a damping that includes recurrences of the correlation function in the VH model, explaining the distinct splitting of the peaks.

B. Quantum Yields, Internal Conversion and Emission Rates

The emission and internal conversion rates for the transitions from initial potential V_i^A are quantified in Figure 11 and used to calculate the fluorescence quantum yield according to Eq. (20). The values are plotted as functions of the of the frequency-domain Gaussian HWHM. The emission rate is basically constant as it is obtained by integration of the whole

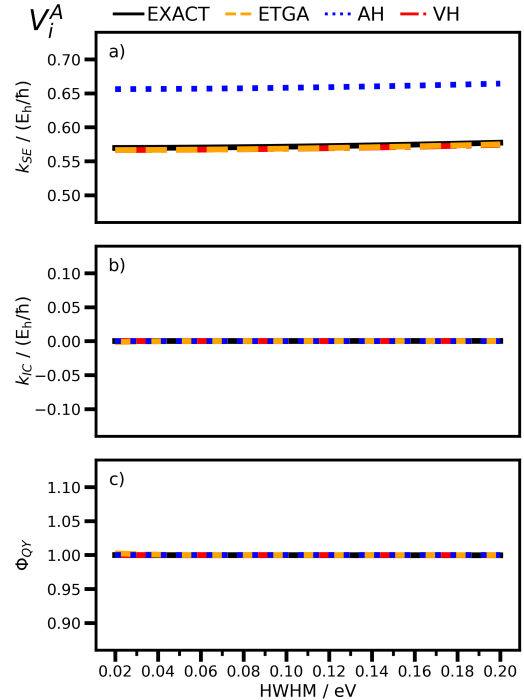


FIG. 11. Spontaneous emission rate (a), internal conversion rate (b) and quantum yield (c) as functions of the HWHM of the applied Gaussian damping function, for the transitions from initial potential V_i^A to a double well potential, calculated using an exact numerical propagation scheme, the ETGA, AH and VH approximation.

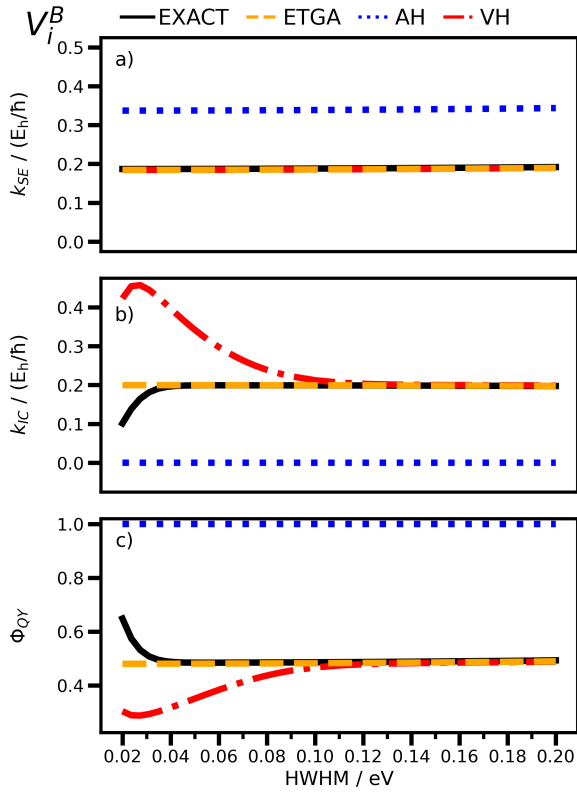


FIG. 12. Spontaneous emission rate (a), internal conversion rate (b) and quantum yield (c) as functions of the HWHM of the applied Gaussian damping function, for the transitions from initial potential V_i^B to a double well potential, calculated using a exact numerical propagation scheme, the ETGA, AH and VH approximation.

emission spectrum, while the internal conversion rate remains fixed at zero since there is no peak near the point of energy conservation that could cause a rise when broadened. The one thing that stands out is the result of the AH model for the emission rate, which is clearly overestimated. The ETGA and the VH model yield the same results for the total emission rate after integration of the spectrum (Fig 8d, 9d).

The results starting from potential V_i^B are given in Figure 12. The emission rate (Fig. 12a) is again invariant to the broadening and the VH and ETGA model yield equivalent results once the spectra are integrated, which are in good agreement with the exact value. But the internal conversion rate (Fig. 12b), which is not obtained by integration but by a single value, shows that there is a regime in which the ETGA method and the vertical harmonic model behave differently. At the lowest values of the HWHM around 0.02 to 0.04 eV, separated individual vibronic states would begin to show. The ETGA method is not capable to model the necessary long time dynamics accurately enough to obtain such a fine resolution in the energy domain and deviates from the exact results in this regime. The vertical harmonic model also predicts a wrong spacing of vibronic states and deviates as well. But the exact result quickly approaches a constant value once the broadening leads to a continuous, overlapping spectrum. The vertical harmonic model also predicts this value in the short-time limit

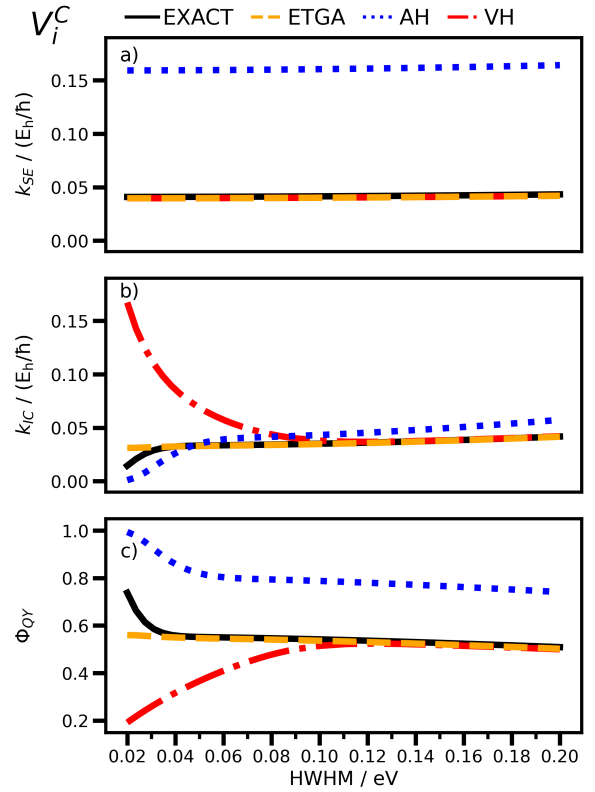


FIG. 13. Spontaneous emission rate (a), internal conversion rate (b) and quantum yield (c) as functions of the HWHM of the applied Gaussian damping function, for the transitions from initial potential V_i^C to a double well potential, calculated using a exact numerical propagation scheme, the ETGA, AH and VH approximation.

that corresponds to a dampening of the correlation function such that only the initial decay matters, beginning approximately at a broadening of 0.1 eV. The adiabatic harmonic model is wrong for all values of broadening and predicts a quantum yield of 1.0 for all values due to an erroneous internal conversion rate of zero.

A similar behaviour is observed for the last case with the transition originating from initial potential V_i^C . The emission rate (Fig. 13a) is again overestimated by the AH model but, unexpectedly, the result for the internal conversion rate (Fig. 13b) is now similar to the exact result for all values of the HWHM. However, a look at the internal conversion spectra given in Figures 8/9c shows that this is only the case due to a crossing of the adiabatic internal conversion spectrum with the exact spectrum at the point of energy conservation at 0.0 eV. The internal conversion spectra indicate that this is a lucky coincidence and the rate value would clearly deviate if the energy shift of the potentials was slightly different, moving the point of energy conservation away from this intersection. The trends in the ETGA and VH model are again the same as in the case before. The ETGA method agrees with the exact results after a small broadening and the VH method converges to the same values as the exact and ETGA model once the broadening corresponds to such a damping in the time domain that only the initial decay of the correlation function matters.

V. CONCLUSION

In this work, the semi-classical Extended Thawed Gaussian Approximation was for the first time applied to predict internal conversion rates. We have illustrated the method's validity and compared its performance with the adiabatic and vertical harmonic models by simulations of internal conversion and emission spectra in increasingly anharmonic potentials, starting with three Morse potentials followed by a double-well potential.

The investigation of the Morse potentials showed the following: The adiabatic harmonic model is capable of treating transitions to the lowest vibrational state, which is sufficient for emission spectra since these transitions usually constitute the largest contribution, also enhanced by the weighting with ω^3 which intensifies peaks at the highest transition energy. But the model is insufficient when it comes to transitions to higher lying vibrational states, which is particularly important for internal conversion.

The ETGA method proves superior and is able to capture effects on the transition amplitudes and frequencies caused by the anharmonicity of the underlying potential. Despite being a clear improvement with respect to harmonic models, it also has difficulties with increasing anharmonicity. Negative peaks and signals at the wrong frequency grow in intensity. The adiabatic model however remains completely oblivious to the growing anharmonicity in the case of the Morse potential, as the only relevant parameter, the second derivative of the potential at the equilibrium, remains constant. The AH model thus predicts the same results for all investigated values of anharmonicities, clearly a big disadvantage.

The vertical harmonic model is not invariant to the changes of anharmonicity and it yields in all cases very good values for the emission rate, as the latter is rather insensitive to the vibrational structure of the integrated emission spectrum as long as the outline and position of the exact spectrum are matched. The vertical harmonic model is capable to do so by capturing the initial decay of the correlation function accurately, but the vibrational structure and the splitting of individual peaks depend on the recurrence time after the initial decay of the correlation function, which cannot be obtained within the VH model. This is a problem if vibrational relaxation or dephasing due to an environment are not sufficiently fast to suppress the vibrational structure, equivalent to a fast damping of the correlation function in the time domain.

The limit of strong damping and a fast decay of the correlation function was considered for the double well potential by applying a Gaussian damping functions with varying width. Differences between the ETGA and the VH results vanish in all cases considered once the damping limits the dynamics to the initial decay, which corresponds roughly to a spectral broadening larger than 0.1 eV in this model. Both methods agree with the exact results in this limit and there is no benefit in using the ETGA over the VH model in this regime. The ETGA method however distinguishes itself from the VH model if the damping is reduced. The vertical harmonic model begins to diverge from the exact results once recurrences within the correlation function are included in

the calculation. The same happens to ETGA model at even weaker damping as it also fails to reproduce the exact long term dynamics, which are required for a high spectral resolution. The adiabatic harmonic model yields the worst results. It generally overestimates the emission rate and values of the internal conversion rate are also unreliable if there is an appreciable energy gap between the potentials.

The AH model might be useful for internal conversion if the initial and final electronic states are almost degenerate in energy. But it cannot be used to model systems that emit at higher energies, entering the range of visible wavelengths, i.e. systems interesting for technical applications such as LEDs. The emission spectrum might be adequate but the internal conversion rate is most certainly wrong, unless the system is perfectly harmonic, in which case all models would predict the same. The vertical harmonic model appears to be a good method if only the initial decay of the correlation function is relevant. This should be the case if vibrational relaxation of the high-lying vibronic states of the final potential is fast, which should be a fair assumption for large polyatomic molecules or systems in contact with a bath that possesses a large density of states. The ETGA method is expected to be an improvement over the VH model if the lifetime of the final states is not too short. This is the case in optical transitions where the bright states are typically low lying vibronic states that have a long lifetime, which is accessible by measurements of the peak width in vibronically resolved spectra, explaining the methods benefits when it comes to absorption or emission spectra. But the lifetime of high-lying vibronic states, which are involved in internal conversion, are not readily available and one typically must make an assumption by choice of the width of the spectral lineshape function. The results showed that benefits of the ETGA are expected to play out in cases with an appreciable lifetime.

A robust and universally applicable method for the prediction of internal conversion rates and ultimately quantum yields is still amiss, but the ETGA is a useful extension to the commonly used harmonic models. Particularly for internal conversion rates in systems where transitions to higher vibrational states are relevant, the predictions are reliable if the anharmonicity is not too high. Even floppy systems can be treated. The vertical harmonic and the ETGA model are expected to yield the same results if the lifetime of vibrational states is very short such that only the initial decay of the correlation function matters. The ETGA is expected to provide better results if the lifetime is long enough such that recurrences need to be included.

The outlook for applications of the method to real molecules is promising. Although it has not been used yet to predict internal conversion rates, the method was already applied to simulate emission spectra of molecular systems.^{66,68} This showed the feasibility of the method for internal conversion rate calculations as the computational cost is almost identical to the cost of emission spectra simulations. The only difference is the need for the first order nonadiabatic coupling element instead of the transition dipole moment. But the same trajectory and the same Hessians can be used in the calculation, making up the biggest computational effort. It should

also be noted that the formalism is also applicable to system in thermal equilibrium and not limited to simulations at absolute zero, meaning that temperature effects can also be included.⁶⁷ The viability of the method was proven in this work and the transfer and application to real molecules is within reach.

CONFLICTS OF INTEREST

There are no conflicts to declare.

ACKNOWLEDGMENTS

We gratefully acknowledge financial support by the Deutsche Forschungsgemeinschaft via grant MI1236/6-1.

DATA AVAILABILITY

The data that support the findings of this study are available from the corresponding author upon reasonable request.

REFERENCES

- J. V. Frangioni, "In vivo near-infrared fluorescence imaging," *Current Opinion in Chemical Biology* **7**, 626–634 (2003).
- S. Kim, Y. T. Lim, E. G. Soltesz, A. M. D. Grand, J. Lee, A. Nakayama, J. A. Parker, T. Mihaljevic, R. G. Laurence, D. M. Dor, L. H. Cohn, M. G. Bawendi, and J. V. Frangioni, "Near-infrared fluorescent type II quantum dots for sentinel lymph node mapping," *Nature Biotechnology* **22**, 93–97 (2003).
- L. Kuang, Q. Chen, E. H. Sargent, and Z. Y. Wang, "[60]fullerene-containing polyurethane films with large ultrafast nonresonant third-order nonlinearity at telecommunication wavelengths," *Journal of the American Chemical Society* **125**, 13648–13649 (2003), PMID: 14599188, <https://doi.org/10.1021/ja0376240>.
- Q. Peng, Y. Niu, Z. Wang, Y. Jiang, Y. Li, Y. Liu, and Z. Shuai, "Theoretical predictions of red and near-infrared strongly emitting x-annulated rylenes," *The Journal of Chemical Physics* **134**, 074510 (2011), <https://doi.org/10.1063/1.3549143>.
- Z. Shuai and Q. Peng, "Organic light-emitting diodes: theoretical understanding of highly efficient materials and development of computational methodology," *National Science Review* **4**, 224–239 (2016), <https://academic.oup.com/nsr/article-pdf/4/2/224/31566777/nww024.pdf>.
- L. Zhang and K. W. Cheah, "Thermally activated delayed fluorescence host for high performance organic light-emitting diodes," *Scientific Reports* **8**, 8832 (2018).
- J. M. Hudson, T. J. H. Hele, and E. W. Evans, "Efficient light-emitting diodes from organic radicals with doublet emission," *Journal of Applied Physics* **129**, 180901 (2021), <https://doi.org/10.1063/5.0047636>.
- Y. Song, B. Li, S. Liu, M. Qin, Y. Gao, K. Zhang, L. Lin, C.-K. Wang, and J. Fan, "Structure–property relationship study of blue thermally activated delayed fluorescence molecules with different donor and position substitutions: theoretical perspective and molecular design," *Journal of Materials Chemistry C* **10**, 4723–4736 (2022).
- H. Wang and M. Thoss, "Multilayer formulation of the multiconfiguration time-dependent hartree theory," *The Journal of Chemical Physics* **119**, 1289–1299 (2003).
- U. Manthe, "A multilayer multiconfigurational time-dependent hartree approach for quantum dynamics on general potential energy surfaces," *The Journal of Chemical Physics* **128**, 164116 (2008).
- Y. Liu, L. Martínez-Fernández, J. Cerezo, G. Prampolini, R. Improta, and F. Santoro, "Multistate coupled quantum dynamics of photoexcited cytosine in gas-phase: Nonadiabatic absorption spectrum and ultrafast internal conversions," *Chemical Physics* **515**, 452–463 (2018), ultrafast Photoinduced Processes in Polyatomic Molecules: Electronic Structure, Dynamics and Spectroscopy (Dedicated to Wolfgang Domcke on the occasion of his 70th birthday).
- J. A. Green, M. Y. Jouybari, D. Aranda, R. Improta, and F. Santoro, "Nonadiabatic absorption spectra and ultrafast dynamics of dna and rna photoexcited nucleobases," *Molecules* **26** (2021), 10.3390/molecules26061743.
- Y. Wang, J. Ren, and Z. Shuai, "Evaluating the anharmonicity contributions to the molecular excited state internal conversion rates with finite temperature TD-DMRG," *The Journal of Chemical Physics* **154**, 214109 (2021).
- J.-j. Ren, Y.-h. Wang, W.-t. Li, T. Jiang, and Z.-g. Shuai, "Time-dependent density matrix renormalization group coupled with n-mode representation potentials for the excited state radiationless decay rate: Formalism and application to azulene," *Chinese Journal of Chemical Physics* **34**, 565–582 (2021), <https://doi.org/10.1063/1674-0068/cjcp2108138>.
- J. C. Tully, "Molecular dynamics with electronic transitions," *The Journal of Chemical Physics* **93**, 1061–1071 (1990).
- R. Mitrić, U. Werner, M. Wohlgenuth, G. Seifert, and V. Bonačić-Koutecký, "Nonadiabatic dynamics within time-dependent density functional tight binding method," *The Journal of Physical Chemistry A* **113**, 12700–12705 (2009).
- M. Barbatti, "Nonadiabatic dynamics with trajectory surface hopping method," *Wiley Interdisciplinary Reviews: Computational Molecular Science* **1**, 620–633 (2011).
- M. I. S. Röhr, J. Petersen, M. Wohlgenuth, V. Bonačić-Koutecký, and R. Mitrić, "Nonlinear absorption dynamics using field-induced surface hopping: Zinc porphyrin in water," *ChemPhysChem* **14**, 1377–1386 (2013).
- J. Hoche, H.-C. Schmitt, A. Humeniuk, I. Fischer, R. Mitrić, and M. I. S. Röhr, "The mechanism of excimer formation: an experimental and theoretical study on the pyrene dimer," *Physical Chemistry Chemical Physics* **19**, 25002–25015 (2017).
- J. P. Malhado, M. J. Bearpark, and J. T. Hynes, "Non-adiabatic dynamics close to conical intersections and the surface hopping perspective," *Frontiers in Chemistry* **2** (2014), 10.3389/fchem.2014.00097.
- G. Cui and W. Thiel, "Generalized trajectory surface-hopping method for internal conversion and intersystem crossing," *The Journal of Chemical Physics* **141**, 124101 (2014).
- W. Xie, M. Sapunar, N. Došlić, M. Sala, and W. Domcke, "Assessing the performance of trajectory surface hopping methods: Ultrafast internal conversion in pyrazine," *The Journal of Chemical Physics* **150**, 154119 (2019).
- T. S. Blacker, R. J. Marsh, M. R. Duchon, and A. J. Bain, "Activated barrier crossing dynamics in the non-radiative decay of nadh and nadph," *Chemical Physics* **422**, 184–194 (2013).
- J. Hoche, A. Schulz, L. M. Dietrich, A. Humeniuk, M. Stolte, D. Schmidt, T. Brixner, F. Würthner, and R. Mitrić, "The origin of the solvent dependence of fluorescence quantum yields in dipolar merocyanine dyes," *Chemical Science* **10**, 11013–11022 (2019).
- H. Kramers, "Brownian motion in a field of force and the diffusion model of chemical reactions," *Physica* **7**, 284–304 (1940).
- A. W. Kohn, Z. Lin, and T. V. Voorhis, "Toward prediction of nonradiative decay pathways in organic compounds i: The case of naphthalene quantum yields," *The Journal of Physical Chemistry C* **123**, 15394–15402 (2019).
- Z. Lin, A. W. Kohn, and T. V. Voorhis, "Toward prediction of nonradiative decay pathways in organic compounds ii: Two internal conversion channels in bodipys," *The Journal of Physical Chemistry C* **124**, 3925–3938 (2020).
- A. Hazra and M. Nooijen, "Derivation and efficient implementation of a recursion formula to calculate harmonic franck-condon factors for polyatomic molecules," *International Journal of Quantum Chemistry* **95**, 643–657 (2003).
- A. Hazra, H. H. Chang, and M. Nooijen, "First principles simulation of the UV absorption spectrum of ethylene using the vertical franck-condon approach," *The Journal of Chemical Physics* **121**, 2125–2136 (2004).
- M. Dierksen and S. Grimme, "An efficient approach for the calculation of franck-condon integrals of large molecules," *The Journal of Chemical Physics* **122**, 244101 (2005).
- F. Santoro, A. Lami, R. Improta, J. Bloino, and V. Barone, "Effective method for the computation of optical spectra of large molecules at finite

- temperature including the duschinsky and herzberg–teller effect: The qx band of porphyrin as a case study,” *The Journal of Chemical Physics* **128**, 224311 (2008), <https://doi.org/10.1063/1.2929846>.
- ³²V. Barone, J. Bloino, M. Biczysko, and F. Santoro, “Fully integrated approach to compute vibrationally resolved optical spectra: From small molecules to macrosystems,” *Journal of Chemical Theory and Computation* **5**, 540–554 (2009).
- ³³J. Bloino, M. Biczysko, F. Santoro, and V. Barone, “General approach to compute vibrationally resolved one-photon electronic spectra,” *Journal of Chemical Theory and Computation* **6**, 1256–1274 (2010).
- ³⁴F. J. A. Ferrer and F. Santoro, “Comparison of vertical and adiabatic harmonic approaches for the calculation of the vibrational structure of electronic spectra,” *Physical Chemistry Chemical Physics* **14**, 13549 (2012).
- ³⁵M. I. Sorour, A. H. Marcus, and S. Matsika, “Modeling the electronic absorption spectra of the indocarbocyanine cy3,” *Molecules* **27**, 4062 (2022).
- ³⁶P. A. M. Dirac, “The quantum theory of the emission and absorption of radiation,” *Proceedings of the Royal Society of London. Series A, Containing Papers of a Mathematical and Physical Character* **114**, 243–265 (1927).
- ³⁷E. Fermi, *Nuclear Physics* (University of Chicago Press, 1950) p. 142.
- ³⁸R. Engelman and J. Jortner, “The energy gap law for radiationless transitions in large molecules,” *Molecular Physics* **18**, 145–164 (1970).
- ³⁹V. G. Plotnikov, “Regularities of the processes of radiationless conversion in polyatomic molecules,” *International Journal of Quantum Chemistry* **16**, 527–541 (1979).
- ⁴⁰R. R. Valiev, R. T. Nasibullin, V. N. Cherepanov, G. V. Baryshnikov, D. Sundholm, H. Ågren, B. F. Minaev, and T. Kurtén, “First-principles calculations of anharmonic and deuteration effects on the photophysical properties of polyacenes and porphyrinoids,” *Physical Chemistry Chemical Physics* **22**, 22314–22323 (2020).
- ⁴¹R. R. Valiev, V. N. Cherepanov, G. V. Baryshnikov, and D. Sundholm, “First-principles method for calculating the rate constants of internal-conversion and intersystem-crossing transitions,” *Physical Chemistry Chemical Physics* **20**, 6121–6133 (2018).
- ⁴²R. R. Valiev, R. T. Nasibullin, V. N. Cherepanov, A. Kurtsevich, D. Sundholm, and T. Kurtén, “Fast estimation of the internal conversion rate constant in photophysical applications,” *Physical Chemistry Chemical Physics* **23**, 6344–6348 (2021).
- ⁴³C. Erker and T. Basché, “The energy gap law at work: Emission yield and rate fluctuations of single NIR emitters,” *Journal of the American Chemical Society* **144**, 14053–14056 (2022).
- ⁴⁴Q. Peng, Y. Yi, Z. Shuai, and J. Shao, “Excited state radiationless decay process with duschinsky rotation effect: Formalism and implementation,” *The Journal of Chemical Physics* **126**, 114302 (2007).
- ⁴⁵Y. Niu, Q. Peng, C. Deng, X. Gao, and Z. Shuai, “Theory of excited state decays and optical spectra: Application to polyatomic molecules,” *The Journal of Physical Chemistry A* **114**, 7817–7831 (2010).
- ⁴⁶M. Hayashi, A. M. Mebel, K. K. Liang, and S. H. Lin, “Ab initio calculations of radiationless transitions between excited and ground singlet electronic states of ethylene,” *The Journal of Chemical Physics* **108**, 2044–2055 (1998).
- ⁴⁷Q. Peng, Y. Niu, Q. Shi, X. Gao, and Z. Shuai, “Correlation function formalism for triplet excited state decay: Combined spin–orbit and nonadiabatic couplings,” *Journal of Chemical Theory and Computation* **9**, 1132–1143 (2013).
- ⁴⁸S. Banerjee, A. Baiardi, J. Bloino, and V. Barone, “Temperature dependence of radiative and nonradiative rates from time-dependent correlation function methods,” *Journal of Chemical Theory and Computation* **12**, 774–786 (2016).
- ⁴⁹K. Miyazaki and N. Ananth, “Singularity-free internal conversion golden-rule rate with application to correlated triplet pair recombination in bipentacenes,” *The Journal of Chemical Physics* **156**, 044111 (2022), <https://doi.org/10.1063/5.0076717>.
- ⁵⁰R. Ianculescu and E. Pollak, “Semiclassical initial value representation study of internal conversion rates,” *The Journal of Chemical Physics* **134**, 234305 (2011).
- ⁵¹C. Lasser and C. Lubich, “Computing quantum dynamics in the semiclassical regime,” *Acta Numerica* **29**, 229–401 (2020).
- ⁵²E. J. Heller, “Time-dependent approach to semiclassical dynamics,” *The Journal of Chemical Physics* **62**, 1544–1555 (1975).
- ⁵³E. J. Heller, “Classical s-matrix limit of wave packet dynamics,” *The Journal of Chemical Physics* **65**, 4979–4989 (1976).
- ⁵⁴E. J. Heller, “The semiclassical way to molecular spectroscopy,” *Accounts of Chemical Research* **14**, 368–375 (1981).
- ⁵⁵E. J. Heller, “Frozen gaussians: A very simple semiclassical approximation,” *The Journal of Chemical Physics* **75**, 2923–2931 (1981).
- ⁵⁶G. A. Hagedorn, “Semiclassical quantum mechanics,” *Communications in Mathematical Physics* **71**, 77–93 (1980).
- ⁵⁷G. A. Hagedorn, “Semiclassical quantum mechanics, IV : large order asymptotics and more general states in more than one dimension,” *Annales de l’I.H.P. Physique théorique* **42**, 363–374 (1985).
- ⁵⁸G. A. Hagedorn, “Raising and lowering operators for semiclassical wave packets,” *Annals of Physics* **269**, 77–104 (1998).
- ⁵⁹M. F. Herman and E. Kluk, “A semiclassical justification for the use of non-spreading wavepackets in dynamics calculations,” *Chemical Physics* **91**, 27–34 (1984).
- ⁶⁰E. Kluk, M. F. Herman, and H. L. Davis, “Comparison of the propagation of semiclassical frozen gaussian wave functions with quantum propagation for a highly excited anharmonic oscillator,” *The Journal of Chemical Physics* **84**, 326–334 (1986).
- ⁶¹A. R. Walton and D. E. Manolopoulos, “A new semiclassical initial value method for franck-condon spectra,” *Molecular Physics* **87**, 961–978 (1996), <https://doi.org/10.1080/00268979600100651>.
- ⁶²R. Ianculescu, J. Tatchen, and E. Pollak, “On-the-fly semiclassical study of internal conversion rates of formaldehyde,” *The Journal of Chemical Physics* **139**, 154311 (2013).
- ⁶³A. Patoz, T. Begušić, and J. Vaníček, “On-the-fly ab initio semiclassical evaluation of absorption spectra of polyatomic molecules beyond the condon approximation,” *The Journal of Physical Chemistry Letters* **9**, 2367–2372 (2018).
- ⁶⁴T. Begušić, A. Patoz, M. Šulc, and J. Vaníček, “On-the-fly ab initio three thawed gaussians approximation: A semiclassical approach to herzberg-teller spectra,” *Chemical Physics* **515**, 152–163 (2018), ultrafast Photoinduced Processes in Polyatomic Molecules: Electronic Structure, Dynamics and Spectroscopy (Dedicated to Wolfgang Domcke on the occasion of his 70th birthday).
- ⁶⁵T. Begušić, M. Cordova, and J. Vaníček, “Single-hessian thawed gaussian approximation,” *The Journal of Chemical Physics* **150**, 154117 (2019).
- ⁶⁶A. Prlj, T. Begušić, Z. T. Zhang, G. C. Fish, M. Wehrle, T. Zimmermann, S. Choi, J. Roulet, J.-E. Moser, and J. Vaníček, “Semiclassical approach to photophysics beyond kasha’s rule and vibronic spectroscopy beyond the condon approximation. the case of azulene,” *Journal of Chemical Theory and Computation* **16**, 2617–2626 (2020).
- ⁶⁷T. Begušić and J. Vaníček, “On-the-fly ab initio semiclassical evaluation of vibronic spectra at finite temperature,” *The Journal of Chemical Physics* **153**, 024105 (2020).
- ⁶⁸T. Begušić, E. Tapavicza, and J. Vaníček, “Applicability of the thawed gaussian wavepacket dynamics to the calculation of vibronic spectra of molecules with double-well potential energy surfaces,” *Journal of Chemical Theory and Computation* **18**, 3065–3074 (2022).
- ⁶⁹S.-Y. Lee and E. J. Heller, “Exact time-dependent wave packet propagation: Application to the photodissociation of methyl iodide,” *The Journal of Chemical Physics* **76**, 3035–3044 (1982).
- ⁷⁰A. Humeniuk, M. Bužančić, J. Hoche, J. Cerezo, R. Mitić, F. Santoro, and V. Bonačić-Koutecký, “Predicting fluorescence quantum yields for molecules in solution: A critical assessment of the harmonic approximation and the choice of the lineshape function,” *The Journal of Chemical Physics* **152**, 054107 (2020).
- ⁷¹D. J. Tannor, *Introduction to Quantum Mechanics: A Time-Dependent Perspective* (University Science Books, 2006).
- ⁷²D. Huber, E. J. Heller, and R. G. Littlejohn, “Generalized gaussian wave packet dynamics, schrödinger equation, and stationary phase approximation,” *The Journal of Chemical Physics* **89**, 2003–2014 (1988).
- ⁷³Y. Zhuang, M. R. Siebert, W. L. Hase, K. G. Kay, and M. Ceotto, “Evaluating the accuracy of hessian approximations for direct dynamics simulations,” *Journal of Chemical Theory and Computation* **9**, 54–64 (2012).
- ⁷⁴J. Franck and E. G. Dymond, “Elementary processes of photochemical reactions,” *Transactions of the Faraday Society* **21**, 536 (1926).
- ⁷⁵E. U. Condon, “Nuclear motions associated with electron transitions in diatomic molecules,” *Physical Review* **32**, 858–872 (1928).

- ⁷⁶G. Herzberg and E. Teller, "Schwingungsstruktur der elektronenübergänge bei mehratomigen molekülen," *Zeitschrift für Physikalische Chemie* **21B**, 410–446 (1933).
- ⁷⁷P. M. Morse, "Diatomic molecules according to the wave mechanics. II. vibrational levels," *Physical Review* **34**, 57–64 (1929).
- ⁷⁸M. Feit, J. Fleck, and A. Steiger, "Solution of the schrödinger equation by a spectral method," *Journal of Computational Physics* **47**, 412–433 (1982).
- ⁷⁹M. D. Feit and J. A. Fleck, "Solution of the schrödinger equation by a spectral method II: Vibrational energy levels of triatomic molecules," *The Journal of Chemical Physics* **78**, 301–308 (1983).
- ⁸⁰M. D. Feit and J. A. Fleck, "Wave packet dynamics and chaos in the hénon–heiles system," *The Journal of Chemical Physics* **80**, 2578–2584 (1984).
- ⁸¹R. Kosloff, "Time-dependent quantum-mechanical methods for molecular dynamics," *The Journal of Physical Chemistry* **92**, 2087–2100 (1988).
- ⁸²W. Siebrand, "Radiationless transitions in polyatomic molecules. i. calculation of franck—condon factors," *The Journal of Chemical Physics* **46**, 440–447 (1967).
- ⁸³M. Bixon and J. Jortner, "Intramolecular radiationless transitions," *The Journal of Chemical Physics* **48**, 715–726 (1968).
- ⁸⁴K. F. Freed, "Irreversible electronic relaxation in polyatomic molecules," *The Journal of Chemical Physics* **52**, 1345–1354 (1970).
- ⁸⁵A. Nitzan and J. Jortner, "Non radiative transition probabilities in the statistical limit," *Theoretica Chimica Acta* **30**, 217–229 (1973).
- ⁸⁶A. Nitzan and J. Jortner, "Electronic relaxation of small molecules in a dense medium," *Theoretica Chimica Acta* **29**, 97–116 (1973).
- ⁸⁷R. R. Valiev, R. T. Nasibullin, V. N. Cherepanov, G. V. Baryshnikov, D. Sundholm, H. Ågren, B. F. Minaev, and T. Kurtén, "First-principles calculations of anharmonic and deuteration effects on the photophysical properties of polyacenes and porphyrinoids," *Physical Chemistry Chemical Physics* **22**, 22314–22323 (2020).